Search for light scalar top quark pair production in the $b\bar{b}\ e^{\mp}\mu^{\pm}\ \widetilde{\nu}\overline{\widetilde{\nu}}$ decay channel in $p\bar{p}$ Collisions at $\sqrt{s} = 1.96$ TeV with the DØ Detector

The DØ Collaboration
URL http://www-d0.fnal.gov
(Dated: March 11, 2006)

This work presents a search for pair production of the lighter supersymmetric partner of the top quark ($\widetilde{t}_1$) in 350 pb^{-1} of $p\overline{p}$ collisions of 1.96 TeV energy in the center of mass, collected by the DØ detector at the Tevatron. A search for decays of $\widetilde{t}_1\ \overline{\widetilde{t}_1} \rightarrow b\bar{b}\ e^{\mp}\mu^{\pm}\ \widetilde{\nu}\overline{\widetilde{\nu}}$ within the Minimal Supersymmetric extension of the Standard Model (MSSM) has been performed. No evidence for excess of events above Standard Model backgrounds has been observed. Limits at 95% C.L. on the $\widetilde{t}_1\ \overline{\widetilde{t}_1}$ production cross section have been calculated and an exclusion plot in the mass ($m_{\widetilde{t}_1}$, $m_{\widetilde{\nu}}$) plane is presented.

Preliminary Results for Winter 2006 Conferences

I. INTRODUCTION

Search for the supersymmetric partner of the top quark is particularly interesting because, within the Minimal Supersymmetric extension of the Standard Model (MSSM), the large top quark mass can induce a large mixing between the superpartners of the left and right helicity states of the top quark and consequently can lead to a substantial mass splitting between the two scalar top mass eigenstates $\widetilde{t_1}$ and $\widetilde{t_2}$. In this scenario the lighter supersymmetric partner of the top quark $\widetilde{t_1}$ can potentially be the lightest scalar quark.

If R-parity is conserved and if $\widetilde{t_1}$ is lighter than the top quark, $\widetilde{t_1}$ may decay either into b quark and on-shell chargino $\widetilde{t_1} \rightarrow b\tilde{\chi}_1^{\pm}$ or into c quark and neutralino $\widetilde{t_1} \rightarrow c\tilde{\chi}_1^{\circ}$. The first decay channel is difficult to explore at the Tevatron due to the high $\tilde{\chi}_1^{\pm}$ mass limit of LEP2 [1]. The second decay channel, already extensively explored, might not be the dominant decay as it proceeds via flavour changing neutral loop diagrams which are highly suppressed. Other possibilities are 3-body decays into $\widetilde{t_1} \rightarrow b\tilde{\ell}\nu$ or into $\widetilde{t_1} \rightarrow b\ell\tilde{\nu}$. The former decay channel is almost closed for most of the stop mass within Tevatron reach, due to the slepton mass limit of LEP2 [1].

The last decay channel however can still be open since $\widetilde{\nu}$ may be relatively light: $m_{\tilde{\nu}} \geq 45$ GeV. This decay channel proceeds via virtual chargino and is expected to yield equal e, μ and τ branching ratios.

At the Tevatron, the scalar top quarks are expected to be produced in pairs in $p\overline{p}$ collisions via gg fusion and $q\overline{q}$ annihilation. Assuming $\widetilde{\nu}$ is the lightest supersymmetric lepton and R parity is conserved, $\widetilde{t_1}$ decay into $\widetilde{t_1} \rightarrow b\ell\tilde{\nu}$ will yield a final state with two oppositely charged leptons, two b jets and a missing transverse energy. Note that $\widetilde{\nu}$ may not be necessarily the LSP since a decay of $\widetilde{\nu} \longrightarrow \nu\chi_1^0$ is experimentally indistinguishable.

In the present analysis we search for a final state with one isolated electron and one isolated muon of opposit electric charges and with significant missing transverse energy. Information on jet activity is included by counting the number of non-isolated charged tracks in the event. Similar search has been performed by DØ using Run-I data [2].

II. DATA AND MONTE CARLO SAMPLES

The analysis presented in this note is based on a data sample collected by the DØ experiment between October 2002 and August 2004 and corresponding to an integrated luminosity of $\mathcal{L}_{\rm int} = 350$ pb^{-1}. The triggers used require a single muon trigger at level 1 and level 2 and one calorimeter trigger tower at the three trigger levels.

Signal events corresponding to $p\overline{p} \rightarrow \widetilde{t_1}\,\overline{\widetilde{t_1}}$ production processes followed by $\widetilde{t_1} \rightarrow b\ell\tilde{\nu}$ ($\ell = e, \mu$) decays via virtual chargino were generated with the CompHEP 4.2p1 program [3] using the parametrization CTEQ5L for the Parton Density Function (PDF) of the p and the $\overline{p}$, and subsequently processed through PYTHIA 6.202 [4]. The MSSM parameters used to obtain the relevant $\widetilde{t_1}$ and $\widetilde{\nu}$ masses and kinematic characteristics of the $\widetilde{t_1}$ decay are the same as those used in the $\widetilde{t_1}\,\overline{\widetilde{t_1}} \rightarrow b\overline{b}\,\mu^+\mu^-\,\widetilde{\nu}\,\overline{\widetilde{\nu}}$ analysis [5]. They are summarized, along with $\widetilde{t_1}$ and $\widetilde{\nu}$ masses and cross sections in Table I.

Background events arise from two independent sources: Physics background events originating from Standard Model (SM) processes with a genuine electron and a genuine muon and neutrino(s) in the final state, namely $Z \rightarrow \tau^+\tau^-$, WW, WZ, ZZ and $t\overline{t}$, and what is called hereafter instrumental background. The latter corresponds to events with a genuine (or fake) electron and a fake (or genuine) muon and neutrino(s) and also events with both fake electron and fake muon and either a genuine or a fake missing transverse energy ($\not\!\!E_T$). These events originate from SM processes $W^+ \rightarrow \ell^+\nu_\ell$ ($\ell = e, \mu, \tau$) + jets, $Z/\gamma^\star \rightarrow \mu^+\mu^-$ + jets, $Z/\gamma^\star \rightarrow e^+e^-$ + jets, $W^+\gamma(W^+ \rightarrow \mu^+\nu_\mu)$ + jets, $Z\gamma(Z \rightarrow \mu^+\mu^-)$ + jets and multijets processes. Physics background events are simulated using PYTHIA [4] MC program except for the $t\bar{t}$ process which was generated with the MC events generator ALPGEN [7] followed by hadronization of the PYTHIA program. Instrumental background however was determined from data itself through the measurement of the electron and the muon fake rates in data samples which are orthogonal to the analysis sample.

III. EVENT SELECTION AND DATA/BACKGROUND COMPARISON

A. Event selection

In each event we require a reconstructed primary vertex within $|z_{vtx}| < 60$ cm and at least one muon candidate of $p_T > 8$ GeV and one electron candidate of $p_T > 12$ GeV, with an electric charge opposit to that of the muon. The criteria used for muon and electron identifications are listed below.

1. Muon identification

Candidate muons are selected using the following criteria:

- wire and scintillator hits in the inner and the outermost layers of the muon detector, matched to the central tracking detector,
- timing cuts to reject cosmic muons,
- at least one hit in the silicon tracker,
- isolation from calorimeter energy: $(E(0.4) - E(0.1) < 2.5)$ GeV, where $E(R)$ is the transverse energy measured in the calorimeter in a radius $R = \sqrt{(\Delta\phi)^2 + (\Delta\eta)^2}$ around the muon,
- isolation from other tracks: $\sum_i^{R=0.5} p_T(i)$ <2.5 GeV, where the sum is over all charged tracks in a cone of radius $R = 0.5$ around the muon.

2. Electron identification

Candidate electrons are selected using the following criteria:

- the ratio of the electromagnetic (EM) energy to the total shower energy should be greater than 0.9,
- isolation from the other energy deposit in the calorimeter: $[E(0.4) - E_{EM}(0.2)]/E(0.2)_{EM}$ <0.15, where $E(R)$ and $E_{EM}(R)$ are respectively the total and the EM energy, deposited in a cone of radius R centered around the electron candidate,
- the lateral and the longitudinal shapes of the EM energy should correspond to those of an electron.

To reduce the contamination from photons and jets faking electrons a likelihood estimator combining information from the energy deposited in the calorimeter and the associated track is used. To select good electrons we require a likelihood value greater than 0.5. Electron candidates are also required to be within $|\eta_{det}| < 1.1$ in the central calorimeter and $1.5 < |\eta_{det}| < 2.5$ in the end-caps to avoid regions where the calorimeter based electron identification variables are poorly measured. Finally we reject electron candidates that share the same track with any good muon candidate in the event. These electron candidates originate from the muon bremstrahlung in which the photon, emitted by the muon, passes the electron identification criteria and is attached to the muon track.

The muon and the electron identification criteria described above along with their p_T cuts and the requirement on the primary vertex will be refered as Cut0 in the rest of the note.

B. Comparison of data with signal and backgrounds

After the selection cuts (Cut0) described in section III A, data and the sum of instrumental and physics backgrounds are compared (Figure 1) as a function of the following variables:

- $\not\!\!E_T$,
- $|\eta_e| + |\eta_\mu|$,
- $S_T = p_T^e + p_T^\mu + \not\!\!E_T$,
- the number of non isolated tracks (NIT) in the event.

The variable NIT is used to characterize the jet activity in the event. It corresponds to the number of tracks in the event other than the leading electron and the leading muon, which have one or more neighbouring tracks in a cone of radius $R = 0.5$ around the tested track. Moreover the tracks in the cone are required to point to the same or neighbouring vertices within 0.01 cm in the z coordinate, and the sum of their p_T is required to be greater than 2.5 GeV.

Also shown in Figures 1 are the expected signal events for signal points A8 and D2 (see Table I), after Cut0.

The number of remaining events in data and from different background processes after Cut0 are summarized in Table II. The errors quoted are statistical only. As can be seen from Table II and from Figure 1, there is a good agreement between data and the sum of the instrumental and the physics backgrounds in both normalization and shape for all variables. The dominating backgrounds at the Cut0 level are the physics process $Z \to \tau^+\tau^-$ and the instrumental background.

TABLE I: Signal points ($m_{\tilde{t}_1}$,$m_{\tilde{\nu}}$) as simulated by CompHEP for tan$\beta = 20$, $\mu = +225$, $M(\tilde{g}) = 500$ GeV, $M(H_A) = 800$ GeV and their varying MSSM parameters A_t, $M_{L_{1,2}}$, and M_1 and M_2, which are respectively the tri-linear scalar mixing term for the top sector, the masses of the left slepton of the two first generation, the U(1) and the SU(2) gaugino masses. The total cross sections (NLO) for the different signal points are obtained from PROSPINO [6] program.

Signal points	A_t [GeV]	$M_{L_{1,2}}$ [GeV]	M_1 [GeV]	M_2 [GeV]	$m_{\tilde{t}_1}$ [GeV]	$m_{\tilde{\nu}}$ [pb]	$\sigma(NLO)\cdot$Br
A1	510.0	82.0	53.5	215	70.63	50.86	21.652
A2	501.5	82.0	53.5	215	80.06	50.86	11.112
A3	480.0	82.0	53.5	210	100.03	50.86	3.309
A4	467.0	82.0	53.5	210	110.36	50.86	1.916
A5	453.0	82.0	53.5	225	120.50	50.86	1.167
A6	438.0	82.0	53.5	225	130.49	50.86	0.741
A7	422.5	82.0	53.5	230	140.07	50.86	0.491
A8	413.0	82.0	53.5	230	145.63	50.86	0.391
A9	405.0	82.0	53.5	250	150.16	50.86	0.326
A10	386.0	82.0	53.5	275	160.39	50.86	0.219
B1	501.5	88.5	63	215	80.06	60.80	11.112
B2	491.2	88.5	63	215	90.18	60.80	5.841
B3	480.0	88.5	63	210	100.03	60.80	3.309
B4	453.0	88.5	63.7	225	120.05	60.80	1.167
B5	422.5	88.5	63.7	230	140.07	60.80	0.491
B6	405.0	88.5	63.7	250	150.16	60.80	0.326
B7	367.0	88.5	63.7	310	170.00	60.80	0.159
C1	491.2	95.5	74	215	90.18	70.60	5.841
C2	480.0	95.5	74	210	100.03	70.60	3.309
C3	438.0	95.5	74	225	130.49	70.60	0.741
C4	422.5	95.5	74	230	140.07	70.60	0.491
C5	405.0	95.5	74	230	150.16	70.60	0.326
D1	480.0	103.0	85	210	100.03	80.45	3.309
D2	467.0	103.0	85	210	110.36	80.45	1.916
D3	453.0	103.0	85	225	120.50	80.45	1.167
D4	438.0	103.0	85	225	130.49	80.45	0.741
D5	422.5	103.0	85	230	140.07	80.45	0.491
D6	405.0	103.0	85	230	150.16	80.45	0.326
D7	367.0	103.0	85	310	170.00	80.45	0.159
E1	467.0	111.0	95.5	210	110.36	90.48	1.916
F1	453.0	119.5	106.5	225	120.50	100.72	1.167
F2	438.0	119.5	106.5	225	130.49	100.72	0.741
F3	422.5	119.5	106.5	230	140.07	100.72	0.491
F4	453.0	119.5	106.5	225	150.16	100.72	0.326

IV. OPTIMUM SEPARATION OF THE SIGNAL FROM THE BACKGROUND

In order to separate the stop signal from the SM background further selection cuts are needed. A first series of cuts labeled in what follows by Cut1 are:

- $\not{E}_T > 15$ GeV,
- $\Delta\phi(e, \not{E}_T) > 0.4$ and $0.4 < \Delta\phi(\mu, \not{E}_T) < 3.0$, where $\Delta\phi(e, \not{E}_T)$ and $\Delta\phi(\mu, \not{E}_T)$ are the differences in the azimuthal angles between the electron and the missing transverse energy and the muon and the missing transverse energy, respectively,
- $M_T(e, \not{E}_T) > 15$ GeV, where $M_T(e, \not{E}_T)$ is the transverse mass of the electron and the missing transverse energy,
- $|z_\mu - z_{PV}| < 3\sigma$, where z_{PV} and z_μ are the z coordinates of the primary vertex and that of the closest point of the muon trajectory to it. The standard deviation σ of $z_\mu - z_{PV}$ has been detemined in $Z \to \mu^+\mu^-$ events sample separately for data and MC from a Gaussian fit of the $z_\mu - z_{PV}$ distribution.

The cuts on $\Delta\phi(e, \not{E}_T)$, $\Delta\phi(\mu, \not{E}_T)$ and $M_T(e, \not{E}_T)$ have been chosen in order to maximize the ratio $S = N_s/\sqrt{N_b}$, where N_s and N_b are the number of expected signal and background events, respectively.

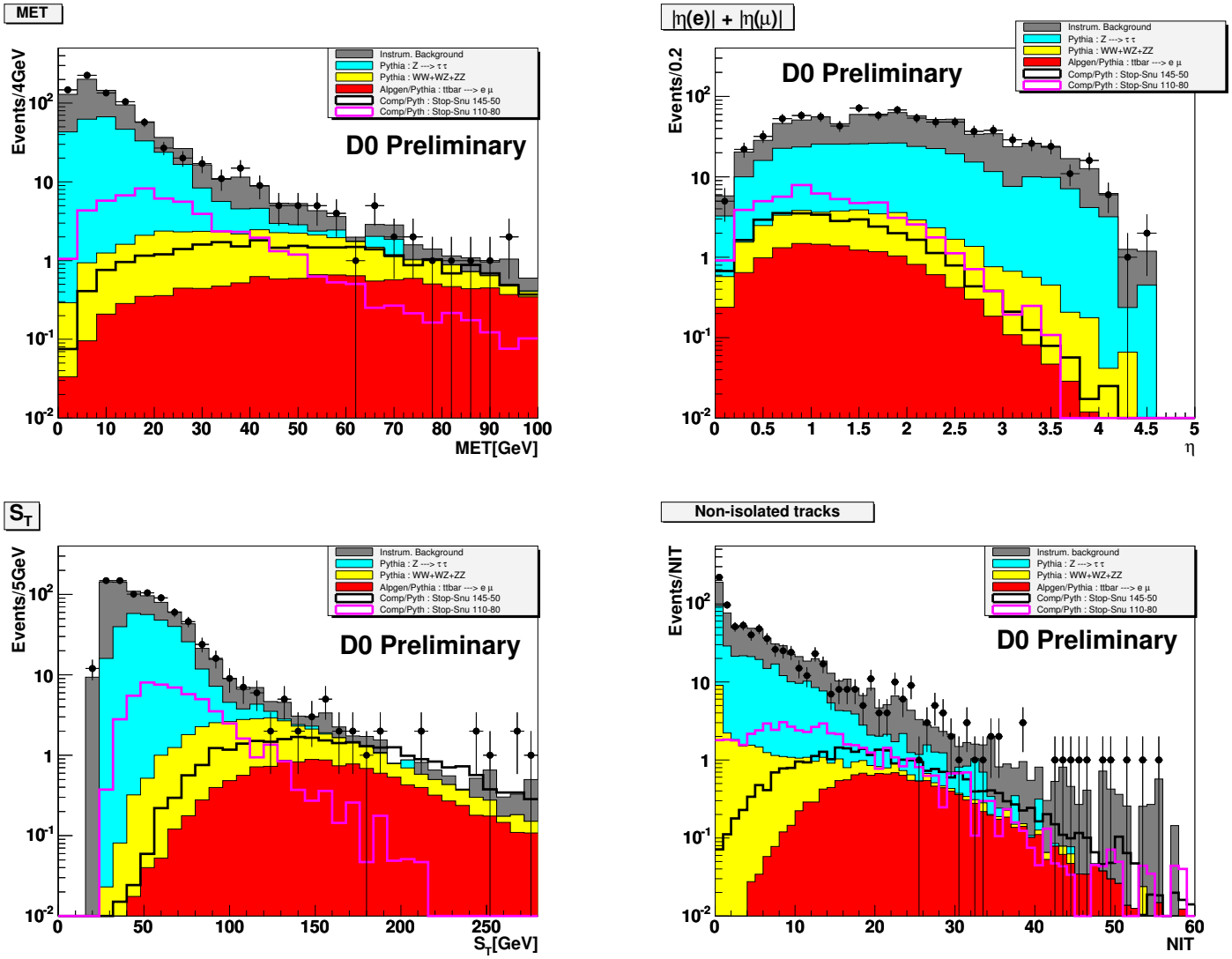

FIG. 1: Distributions after Cut0 of the $\not\!\!E_T$ and $|\eta_e| + |\eta_\mu|$ (upper plots) and $S_T = p_T^e + p_T^\mu + \not\!\!E_T$ and the non-isolated charged track distributions (lower plots) for data (points) and the sum of all backgrounds (histograms) overlaid with MC signal (black and purple lines) corresponding to signal points A8 and D2 of ($m_{\tilde{t}_1}$,$m_{\tilde{\nu}}$) plane.

The number of remaining events in data and from different background processes after these cuts are summarized in Table II. As can be seen the $Z \to \tau^+\tau^-$ and instrumental backgrounds contributions have been suppressed dramatically after Cut1, whereas signal points D2, D4 and A8 corresponding to different $\Delta M = m_{\tilde{t}_1} - m_{\tilde{\nu}}$ values have been reduced moderately.

To minimize the average cross section upper limit expected in the absence of signal events, two additional cuts have been used, labeled in what follows Cut2 and enumerated in Table III. As one can see the cut values have been varied in three different regions of ΔM. This variation of cut values is motivated by the fact that backgrounds from different sources contribute differently in regions of different ΔM values. The number of data and background events along with the number of expected signal events for signal points in the three ΔM regions, obtained after having applied Cut2 are shown in Table II.

V. LIMIT ON THE PRODUCTION CROSS SECTION

Since after the optimization procedure outlined above the number of data events is compatible with the expected number of background and no enhancement for possible signal is observed, we have determined the upper limits of the signal cross sections at 95% confidence level for the generated signal points shown in Table I. We used the modified

TABLE II: Expected number of background and signal events (signal points D2, D4 and A8) for an integrated luminosity of 350 pb^{-1} and number of remaining events in data after cuts: Cut0, Cut1 and Cut2 (see section IV for Cut1 and Cut2 definitions) for the three ΔM =$m_{\tilde{t}_1}$ − $m_{\tilde{\nu}}$ regions. Di-bosons corresponds to the sum of WW, ZZ and WZ contributions. The errors quoted are statistical only.

	$t\bar{t}$	di-bosons	$Z/\gamma^* \to \tau^+\tau^-$	Instrum. bkg	$\sum$(Phys+Instrum) bkg	data
Cut0	13.57 ± 0.18	27.82 ± 0.79	299.40 ± 7.91	438.20 ± 20.93	778.90 ± 22.40	807
Cut1	9.82 ± 0.15	20.18 ± 0.67	12.73 ± 1.62	36.37 ± 6.03	79.10 ± 6.28	80
Cut2a ($20 \leq \Delta M \leq 40$ GeV)	4.34 ± 0.10	7.56 ± 0.41	2.08 ± 0.65	9.00 ± 3.00	22.99 ± 3.10	21
Cut2b ($50 \leq \Delta M \leq 60$ GeV)	5.73 ± 0.11	11.10 ± 0.50	2.97 ± 0.78	14.84 ± 3.85	34.63 ± 3.96	34
Cut2c ($\Delta M \geq 70$ GeV)	6.46 ± 0.12	12.76 ± 0.53	3.20 ± 0.81	18.24 ± 4.27	40.66 ± 4.38	42
	D2	D4	A8			
Cut0	54.59 ± 2.01	41.76 ± 1.14	30.78 ± 0.72			
Cut1	27.12 ± 1.39	25.88 ± 0.87	22.08 ± 0.59			
Cut2a ($20 \leq \Delta M \leq 40$ GeV)	16.43 ± 1.07					
Cut2b ($50 \leq \Delta M \leq 60$ GeV)		18.28 ± 0.72				
Cut2c ($\Delta M \geq 70$ GeV)			16.70 ± 0.51			

TABLE III: Rejection $R_{t\bar{t}}$, $R_{di-boson}$, R_τ, R_{inst}, and reduction R_{D2}, R_{D4}, R_{A8} factors of physics and instrumental backgrounds and the three signal reference points with respect to cuts Cut2a-c. The two cuts on the variables $\Delta\phi(e, \not{E}_T) + \Delta\phi(\mu, \not{E}_T)$ and $|\eta_e| + |\eta_\mu|$ are applied separately in the three ΔM regions.

$\Delta M = m_{\tilde{t}_1}$-$m_{\tilde{\nu}}$	Cut 2		Rejection/reduction factors						
	$\Delta\phi(e, \not{E}_T) + \Delta\phi(\mu, \not{E}_T)$	$\lvert\eta_e\rvert + \lvert\eta_\mu\rvert$	$R_{t\bar{t}}$	$R_{di-boson}$	R_τ	R_{inst}	R_{D2}	R_{D4}	R_{A8}
$20 \leq \Delta M \leq 40$ GeV	> 2.9 & < 4.6	< 1.70	2.26	2.67	6.12	4.04	1.65		
$50 \leq \Delta M \leq 60$ GeV	> 2.8	< 1.70	1.71	1.82	4.29	2.45		1.42	
$\Delta M \geq 70$ GeV	> 2.8	< 1.90	1.52	1.58	3.98	1.99			1.32

frequentist approach and the program TLimit [8] on the topological variables $S_T = p_T^e + p_T^\mu + \not{E}_T$ and NIT which were not involved in the optimization procedure. The distribution of these two variables at the Cut2 level, for two extreme ΔM regions ($\Delta M \simeq 20$ GeV and $\Delta M \geq$70 GeV) are presented in Figures 2. As one can see the signal events behave, in these variables, differently in different ΔM regions. To take advantage of this behaviour, the variable S_T has been divided in the following 3 intervals: $20 \leq S_T \leq 60$ GeV, $60 < S_T \leq 130$ GeV, and $S_T > 130$ GeV and in each S_T interval we have distinguished 3 bins in NIT: $0 \leq$NIT≤ 1, $2 \leq$NIT≤ 8 and NIT> 8.

A. Studies and estimates of systematic effects

Besides the error on the luminosity determination which amounts to 6.5%, the other sources of systematic errors affecting this analysis are:

- uncertainty due to the Jet Energy Scale (JES) error,
- uncertainty in the determination of the instrumental background,
- uncertainties affecting triggers and electron and muon identification efficiencies,
- uncertainties on SM background cross sections due in particular to the proton PDF,
- uncertainties on electron, muon and jet MC resolution,
- uncertainty on the p_T distribution of the $Z \to \ell\ell$ processes,
- discrepancy between data and MC in the number of non isolated tracks.

The systematic errors resulting from the uncertainties on the quantities listed above (except the instrumental background and the NIT) are obtained by varying sequentially each affected quantity within $\pm 1\sigma$ before any cuts are applied. The systematic error on the instrumental background was derived from the difference between the number of instrumental background events obtained with two different control data samples orthogonal to the analysis sample. The systematic error on NIT is determined from the difference between data and MC in the $Z \to \mu^+\mu^-$ sample in

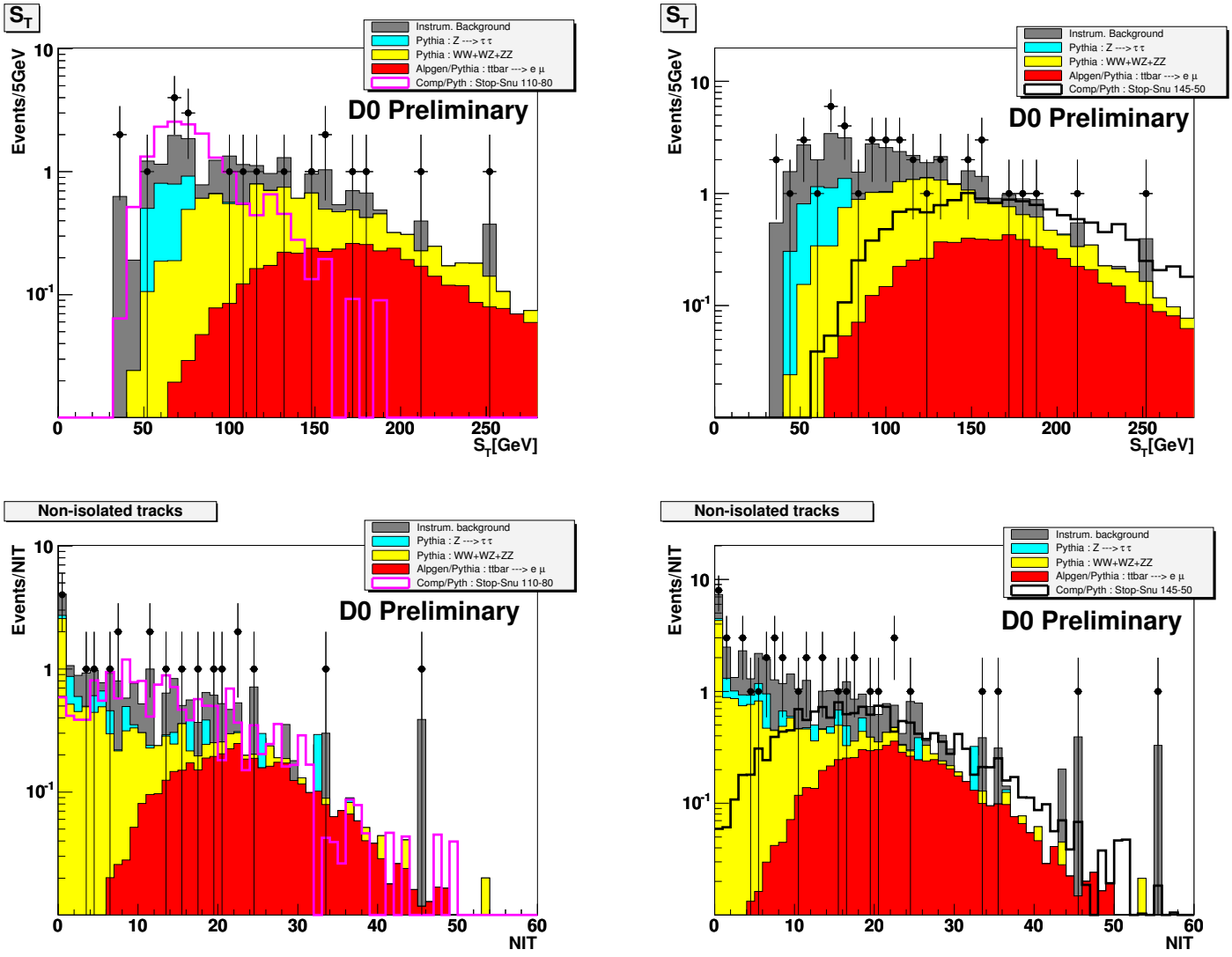

FIG. 2: S_T (upper plots) and NIT (lower plots) distributions for data and the sum of all backgrounds after Cut2 for two ΔM = $m_{\tilde{t}_1}$-$m_{\tilde{\nu}}$ regions: $\Delta M \simeq 20$ GeV (left) and $\Delta M \geq 70$ GeV (right). Signal points corresponding to these two ΔM regions are also displayed.

each NIT bin used in the TLimit package. Table IV presents the systematic errors resulting from the uncertainties on the quantities listed above.

B. Results

Figure 3 shows the region in the $m_{\tilde{\nu}}$ *vs* $m_{\tilde{t}_1}$ plane where the upper limits of the cross sections at the 95% CL are smaller than the signal cross sections calculated at NLO [6]. These latters are taken at their minimum values obtained by changing the renormalization scale by one standard deviation of its uncertainty. As one can see this region considered as excluded, is significantly extended with respect to that obtained in Tevatron Run I.

TABLE IV: Systematic errors. For NIT the systematic errors concern physics backgrounds and signal points only.

		Systematic errors (%) on physics and instrumental backgrounds	Signal points A8	Signal points D2
JES		1	1.5	0.2
Instrumental background		3.3		
Triggers + e and μ id efficiencies		2.0	1.7	2.5
SM cross sections (PDF)		2		
e and μ MC smearing		$\ll 1$	$\ll 1$	$\ll 1$
$Z \to \ell\ell$ pT reweighting		1		
NIT:	≤ 1	1.4	1.4	
	ϵ [2, 8]	3.5	3.5	
	> 8	0.7	0.7	

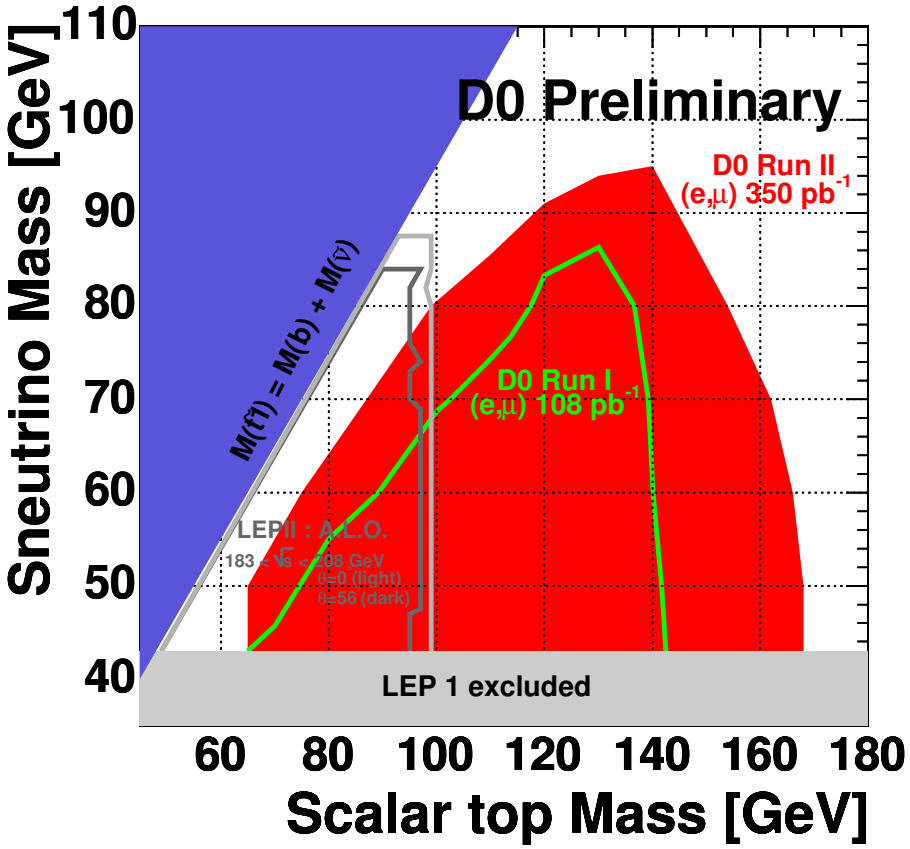

FIG. 3: Region of $\widetilde{t}_1$ and $\widetilde{\nu}$ masses exluded in the present analysis (red area). Also shown are excluded area by D0-RunI data [2] and at LEPI and LEPII [1].

Acknowledgments

We thank the staffs at Fermilab and collaborating institutions, and acknowledge support from the DOE and NSF (USA); CEA and CNRS/IN2P3 (France); FASI, Rosatom and RFBR (Russia); CAPES, CNPq, FAPERJ, FAPESP and FUNDUNESP (Brazil); DAE and DST (India); Colciencias (Colombia); CONACyT (Mexico); KRF and KOSEF (Korea); CONICET and UBACyT (Argentina); FOM (The Netherlands); PPARC (United Kingdom); MSMT (Czech Republic); CRC Program, CFI, NSERC and WestGrid Project (Canada); BMBF and DFG (Germany); SFI (Ireland); The Swedish Research Council (Sweden); Research Corporation; Alexander von Humboldt Foundation; and the Marie Curie Program.

---

[1] http://lepsusy.web.cern.ch/lepsusy/www/squarks_summer04/stop_combi_208_final.html
[2] The DØ Collaboration, "Search for 3- and 4-Body Decays of the Scalar Top Quark in $p\bar{p}$ Collisions at $\sqrt{s} = 1.8$ TeV", Phys. Lett. B 581, 147 (2004).
[3] "CompHEP- a package for evaluation of Feynman diagrams and integration over multi-particle phase space", A. Pukhov *et al.*, INP-MSU 98-41/542 and hep-ph/9908288.
[4] T. Sjöstrand, Comp. Phys. Comm 82, 74, (1994).
[5] DØ Collaboration , DØ Note 4866-Conf.
[6] "PROSPINO, a program for the PROduction of Supersymmetric Particles In Next-to-leading Order QCD", W. Beenacker, R. Hoepker, M. Spira, hep-ph/9611232.
[7] M.L. Mangano *et al.* hep-ph/0206293 and JHEP 0307:001,2003.
[8] T. Junk, NIM A434, 435 (1999).